Materials Research Letters

ISSN: 2166-3831 (Online) Journal homepage: www.tandfonline.com/journals/tmrl20

Single-crystal growth of a FeCoCrMnAl high-entropy alloy

M. Feuerbacher, E. Würtz, A. Kovács & C. Thomas

To cite this article: M. Feuerbacher, E. Würtz, A. Kovács & C. Thomas (2017) Single-crystal growth of a FeCoCrMnAl high-entropy alloy, Materials Research Letters, 5:2, 128-134, DOI: 10.1080/21663831.2016.1234516

To link to this article: https://doi.org/10.1080/21663831.2016.1234516

© 2016 The Author(s). Published by Informa UK Limited, trading as Taylor & Francis Group.

Published online: 20 Sep 2016.

Submit your article to this journal

Article views: 3469

View related articles

View Crossmark data

Citing articles: 3 View citing articles

Full Terms & Conditions of access and use can be found at
https://www.tandfonline.com/action/journalInformation?journalCode=tmrl20

MATER. RES. LETT., 2017
VOL. 5, NO. 2, 128–134
http://dx.doi.org/10.1080/21663831.2016.1234516

MATERIALS RESEARCH LETTERS
Taylor & Francis
Taylor & Francis Group

ORIGINAL REPORT

OPEN ACCESS

Single-crystal growth of a FeCoCrMnAl high-entropy alloy

M. Feuerbacher, E. Würtz, A. Kovács and C. Thomas

Peter Grünberg Institut PGI-5 and Ernst Ruska-Centrum, Forschungszentrum Jülich GmbH, Jülich, Germany

ABSTRACT

We report on single-crystal growth of the equiatomic FeCoCrMnAl high-entropy alloy by means of the Bridgman technique. Our crystals are about 1 cm in diameter and 6.6 cm in length. X-ray Laue images taken at various positions on their surface are sharp and mutually consistent. The material has a microstructure consisting of B2 inclusions in a body-centred cubic matrix. The inclusions are {0 0 1} platelets of about 65 nm thickness with varying lateral extensions of the order of 500 nm, predominantly containing Al and Co. The matrix is rich in Fe and Cr.

IMPACT STATEMENT

We report the growth of a cubic-centimetre-sized single crystal of a high-entropy alloy. We characterize a Bridgman crystal of the equiatomic FeCoCrMnAl phase and analyse its two-phase structure.

ARTICLE HISTORY
Received 19 August 2016
Accepted 5 September 2016

KEYWORDS
High-entropy alloys; single-crystal growth; Bridgman technique; transmission electron microscopy

High-entropy alloys (HEAs) constitute a novel field in materials science, increasingly attracting research interest. Yeh [1] was the first to forward the basic idea to study alloys composed of multiple principal elements, solidifying as metallic solid solutions on a simple crystal lattice. Usually, these alloys contain 4–9, occasionally up to 20 components [2]. As yet, several alloy systems in which HEAs exist have been reported, and HEAs with body-centred cubic (bcc), face-centred cubic (fcc), and hexagonal [3] structures have been found.

In this paper, we report on the single-crystal growth of an HEA. We approached the system FeCoCrMnAl, in which Pradeep et al. recently discovered a novel HEA phase [4]. In the literature, there exists only one previous article addressing single-crystal growth of an HEA [5]. The single crystal described in that paper, however, was fairly small, having a volume of about 0.35 cm^3. In the present paper, we explicitly address the growth of single crystals above a critical volume of 1 cm^3, which allows for the provision of single-crystalline samples for experimental techniques demanding large sample volumes such as e.g. neutron diffraction.

Single-crystal growth was carried out according to the Bridgman technique. An equiatomic melt of high-purity elements Fe, Co, Cr, Mn, and Al was remelted several times in order to ensure homogenization, and eventually cast into a conical mould. The ingot is fitted in a cylindrical, slightly tapered alumina crucible of about 9 cm length and an internal diameter between 9 and 11 mm. The crucible is inserted in a molybdenum tube acting as a susceptor for high-frequency heating and placed on a moveable rod equipped with a cold finger to create a defined and steep temperature gradient. At the beginning of the growth process, the crucible is fully inserted into the susceptor. The temperature is measured pyrometrically through holes drilled into the susceptor tube. In the lower part of the crucible the temperature is set to 1530°C and kept constant during the growth process. Since the liquidus temperature (determined using a Setaram Labsys DSC16) of the material is about 1400°C, the entire ingot is initially molten and the overheating leads to further homogenization of the melt.

Solidification is effected by lowering the crucible relative to the susceptor, that is, by slowly moving the melt

CONTACT M. Feuerbacher m.feuerbacher@fz-juelich.de Peter Grünberg Institut PGI-5 and Ernst Ruska-Centrum, Forschungszentrum Jülich GmbH, D-52425 Jülich, Germany

© 2016 The Author(s). Published by Informa UK Limited, trading as Taylor & Francis Group.
This is an Open Access article distributed under the terms of the Creative Commons Attribution License (http://creativecommons.org/licenses/by/4.0/), which permits unrestricted use, distribution, and reproduction in any medium, provided the original work is properly cited.

out of the hot zone, starting with the tip. Based on our previous experience on the growth of complex metallic alloys, the lowering velocity was chosen as 5 mm/h. The growth process is carried out under argon atmosphere of 650 mbar.

After a first visual inspection, the extension of the single grains and the primary orientation are determined using a Philips Mikro X-ray Laue apparatus in back-reflection geometry. The images are collected digitally using a Photonic Science X-ray Laue Imaging System. For further characterization, slices perpendicular to the [0 1 1] direction are extracted from the crystal by means of spark erosion. Scanning electron microscopy (SEM) is carried out using a JEOL 840 microscope, equipped with an EDAX energy-dispersive X-ray (EDX) system. Sample preparation for transmission electron microscopy (TEM) is carried out by subsequent grinding, dimpling and argon-ion milling, and by focused Ga ion-beam preparation in a dual-beam FEI Helios Nanolab 400S focused ion-beam [6] system. TEM is performed using a Philips CM20 transmission electron microscope operated at 200 kV. High-resolution scanning transmission electron microscopy (STEM) is carried out using a FEI Titan G2 80-200 equipped with a high-angle annular dark-field (HAADF) detector used at a semi-angle of 69 mrad, and an in-column Super-X EDX unit [7].

Figure 1(a) shows a FeCoCrMnAl Bridgman crystal grown mounted on a goniometer head, and from several directions for an overview of its entire surface in Figure 1(b). Its outer appearance corresponds to the inner shape of the alumina crucible. The length of the crystal is 6.6 cm, the diameter is 11 mm at the bottom and 9 mm at the top, that is, its total volume amounts to 5.1 cm^3. On its surface a number of small cavities are visible.

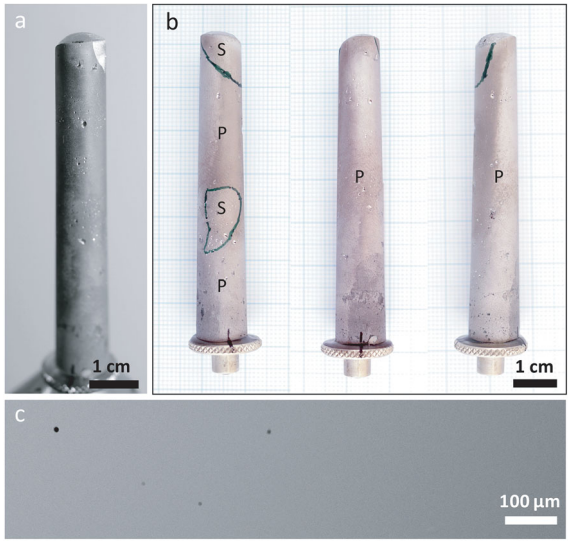

Figure 1. (a) Photograph of a FeCoCrMnAl Bridgman crystal grown mounted on a goniometer head. The tip of the crystal oriented such that a small grain in the upper-right corner is oriented in a specular direction, thus appearing bright. (b) Photographs of the grown crystal from several directions, so that its entire surface can be seen. The grain boundaries are marked on the surface. (c) SEM micrograph of the material using a backscattered-electron detector.

The surface of the crystal is covered with micro-facets causing specular light reflection, which results in a brighter or darker appearance depending on the orientation of the grain relative to the incident light. Figure 1(a) shows the crystal in an orientation, where a small grain in the upper-right corner is seen at a specular direction, thus appearing bright in the photograph, while the rest of the crystal appears darker. Accordingly, visual inspection by rotating the crystal under incident light allows for a first judgment of the extension of the grains and/or the presence of secondary grains.

The grain boundaries located according to visual inspection are drawn on the surface using a marker pen in Figure 1(b). The whole crystal consists of three grains: in the upper part, a small wedge-shaped grain is present, and in its centre we find another irregularly shaped grain. These secondary grains are marked 'S' in Figure 1(b). For the entire remaining bulk, marked 'P', no changes in the appearance of the specular reflection are seen, suggesting that it consists of one large single grain. We will refer to this part as the primary grain of the crystal.

Figure 1(c) is a SEM image of a slice from the FeCoCrMnAl Bridgman crystal recorded using a composition-sensitive backscattered-electron detector. On this length scale, the sample appears perfectly homogeneous. There are no composition variations and no dendrites, and no precipitates or secondary phases can be seen. A few dark spots on the image are visible, which are due to small pores that are present in the crystal. According to our SEM investigations, we estimate the porosity of the crystal to be about 10^{-2}% in the centre and about three times higher in the surface-near region. EDX analysis averaged over the surface area reveals that the overall composition of the crystal grown is $Fe_{21.1}Co_{20.3}Cr_{21.2}Mn_{15.4}Al_{22.0}$. This is close to the nominal equiatomic composition, albeit some Mn, which is the element with the highest vapour pressure, was lost due to evaporation during the growth process.

Figure 2 depicts a series of X-ray Laue diffraction patterns taken from the primary grain (represented using an inverted greyscale for better clarity). The crystal was rotated on a goniometer and the Laue patterns were captured from the resulting different surface positions. All Laue patterns show sharp singular spots, and are consistent concerning their relative tilting angles. Figure 2(a) is the fourfold pattern of the (1 0 0) plane. Figure 2(b) is the twofold pattern of the (0 1 −1) plane and Figure 2(c) the

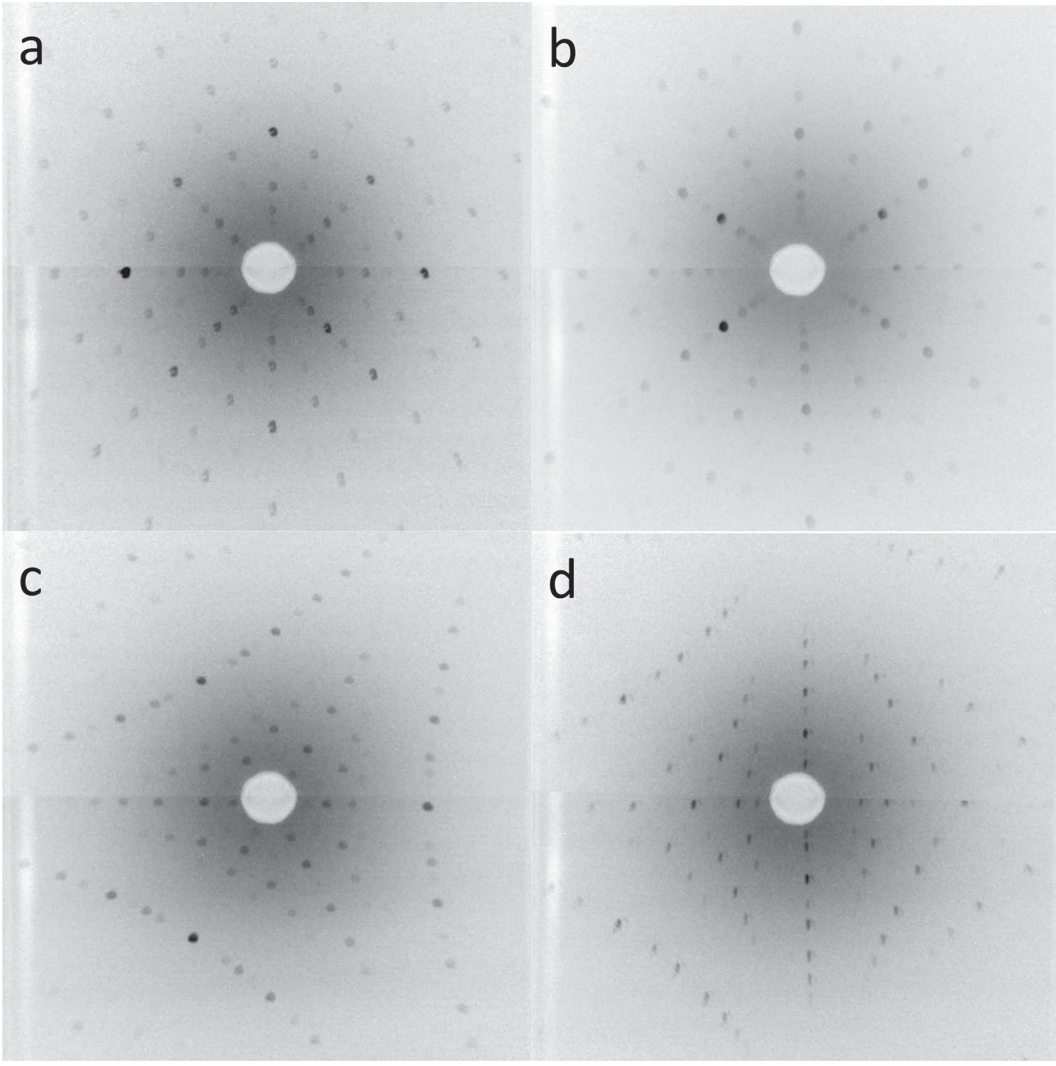

Figure 2. Back-reflection Laue patterns taken in the centre of the primary grain. (a) (1 0 0) plane. (b) (0 1 −1) plane. (c) (1 1 −1) plane. (d) (2 1 −1) plane. The images are represented using an inverted greyscale for better clarity.

threefold pattern of the (1 1 −1) plane, which are tilted by 90° and 55° with respect to (1 0 0), and 35° with respect to each other. Finally, Figure 2(d) shows the pattern of the (2 1 −1) plane, which was obtained by tilting the crystal by 35° with respect to (1 0 0). The long axis of the crystal, that is, the growth direction, is tilted by about 14° with respect to the [0 1 1] direction.

In order to verify our conclusions on the grain structure from the visual inspection, Laue patterns from various positions on the crystal surface were taken. The crystal was oriented to show the (1 0 0) Laue pattern (Figure 2(a)) and then linearly translated with respect to the X-ray beam. We obtain the same diffraction pattern from all spots on the surface from top to bottom over a distance of more than 60 mm. Additionally, we have taken diffraction patterns in the opposite direction from the opposite side of the crystal, which also showed the same characteristic pattern of the (1 0 0) plane. These results confirm our conclusions from the visual inspection—the large crystal region marked 'P' in Figure 1(b) corresponds to an extended single primary grain. Further Laue images taken within the areas marked 'S' demonstrate that these indeed correspond to secondary grains, which are oriented at arbitrary angles with respect to the primary grain. The images of the Laue inspection described are provided in [8].

The volume of the wedge-shaped secondary grain at the top of the crystal can directly be determined as about 0.24 cm^3. Assuming that the visible edges of the secondary grain in the centre of the crystal are straightly connected, its volume can be estimated as 0.07 cm^3. Hence, the volume of the primary grain is as large as 4.8 cm^3.

Figure 3 shows selected-area electron diffraction patterns taken by the transmission electron microscope. The area contributing to diffraction is about 1 μm^2.

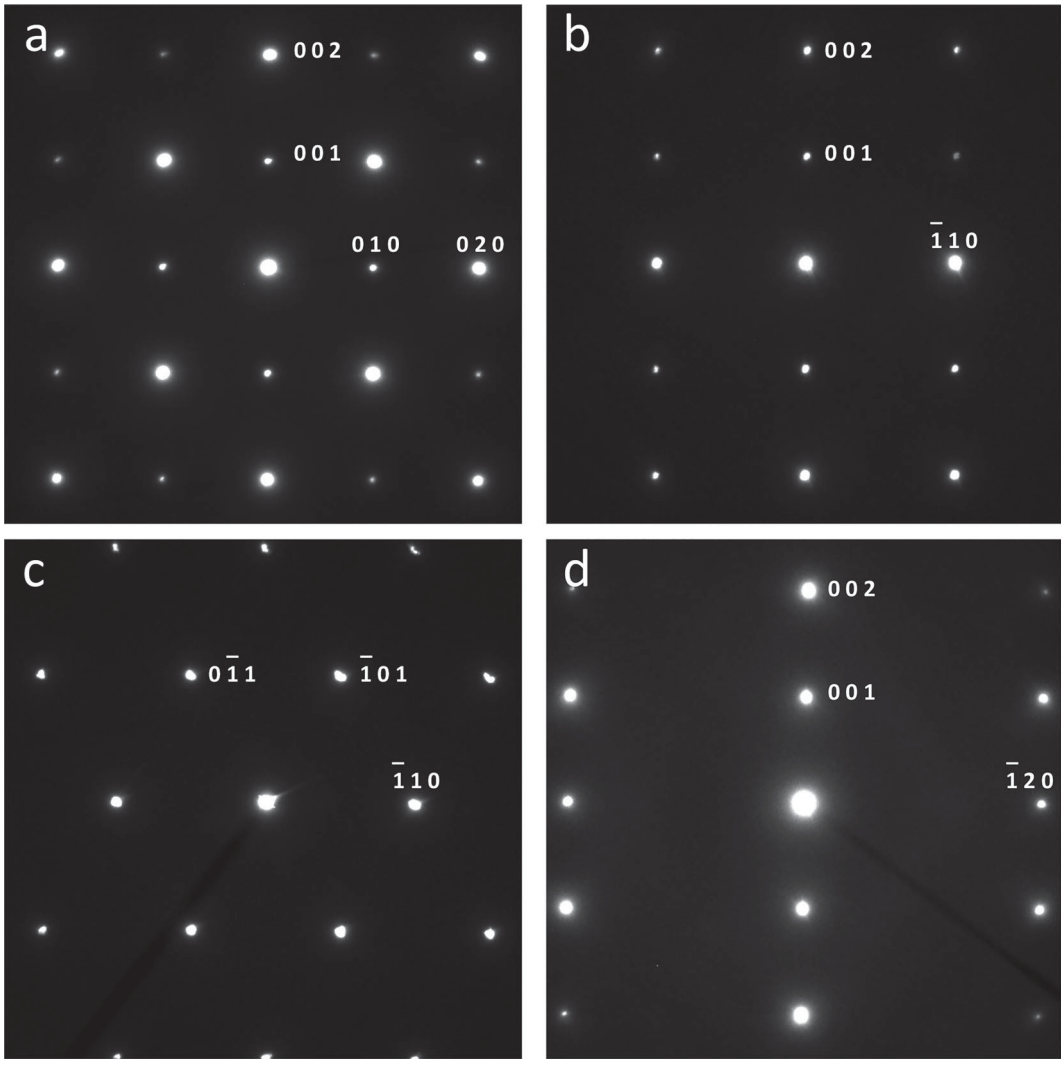

Figure 3. Selected-area diffraction patterns taken in the TEM. (a) [1 0 0] zone axis. (b) [1 1 0] zone axis. (c) [1 1 1] zone axis. (d) [2 1 0] zone axis. Some reflections are indexed.

Diffraction patterns corresponding to the [1 0 0], [1 1 0], [1 1 1], and [2 1 0] zone axes are shown in panels (a–d), respectively. In the [1 0 0], [1 1 0], and [2 1 0] patterns, the presence of {0 0 1} reflections is clearly visible. These reflections are forbidden in the bcc structure and reveal that the material contains B2 structure.

Figure 4(a,b) shows bright-field TEM micrographs taken close to the [1 1 0] zone axis with the reflections (0 0 1) and (0 0 2) simultaneously excited. The images display the typical microstructure of the material on the submicron scale. The material consists of a matrix and inclusions, both existing at an approximately equal volume fraction. The inclusions are elongated and extend along the [0 0 1] and [1 −1 0] directions. While the length of the inclusions varies strongly, their width is rather uniform. Averaging over 20 randomly chosen inclusions, we find a mean width of 63.5 nm for those extending along the [1 −1 0] direction, and of 90.8 nm for those extending along [0 0 1]. Imaged along a $<1\,0\,0>$ direction the microstructure has a similar appearance and all inclusions show the smaller width. We thus conclude that the inclusions are {0 0 1} platelets of about 65 nm thickness. Their lateral extensions vary and are of the order of 500 nm.

Figure 4(c) is a dark-field TEM micrograph using the (0 0 1) reflection of the exact area shown in Figure 4(b). Under these conditions the inclusions are bright while the matrix is dark. The (0 0 1) reflection is present in the B2 structure but forbidden in the bcc structure. Hence, we can conclude that the inclusions possess the B2 structure, while the matrix is bcc. These conclusions are confirmed by high-resolution STEM. Figure 4(d) is a micrograph taken along the [1 1 0] direction with a Z-contrast-sensitive HAADF detector. The upper part of the image corresponds to the matrix area, the lower part to an inclusion. The phase boundary is located in the

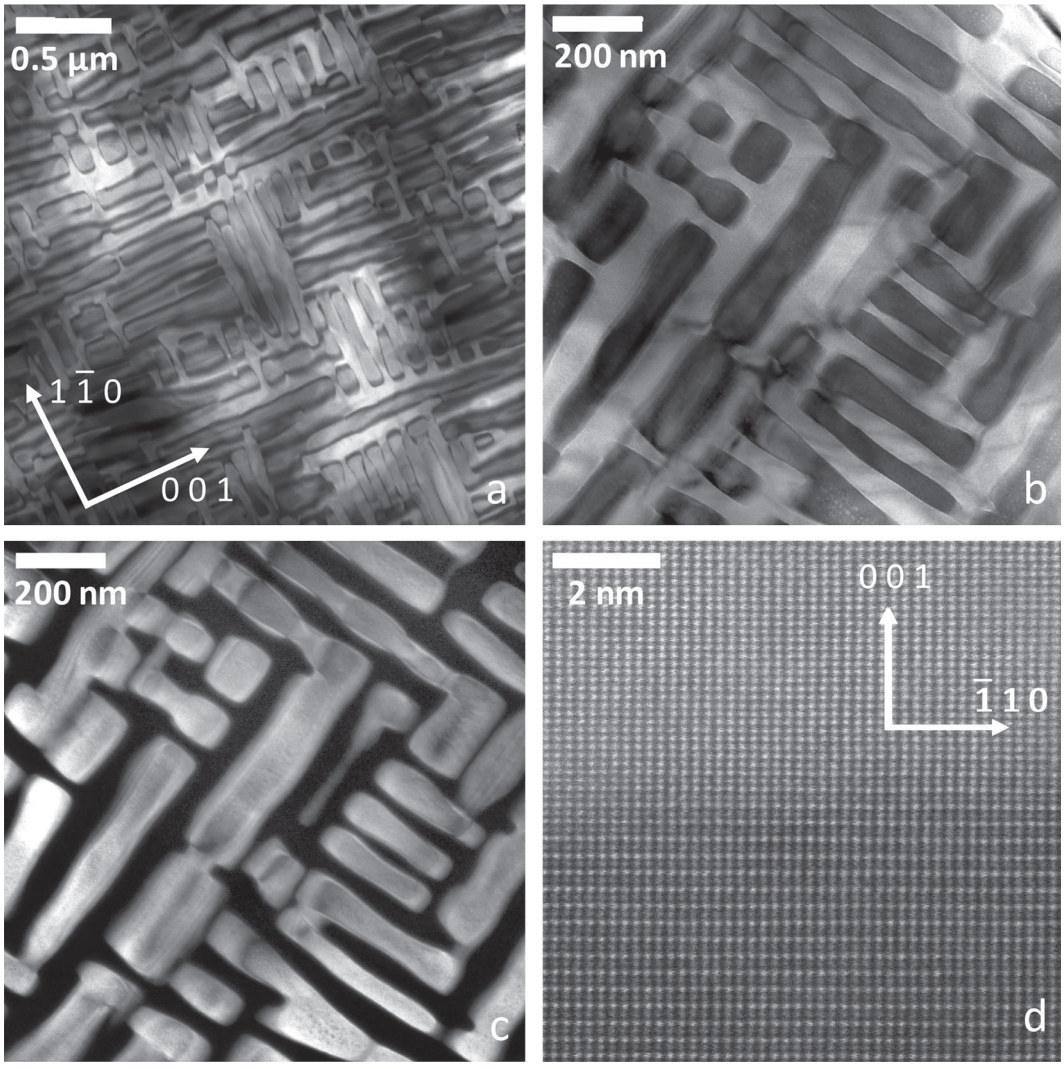

Figure 4. (a and b) Bright-field TEM micrographs taken close to the [1 1 0] zone axis displaying the typical microstructure with the reflections (0 0 1) and (0 0 2) simultaneously excited. (c) Dark-field image of the region shown in (b) using the (0 0 1) reflection. (b) High-resolution HAADF STEM micrograph along the [1 1 0] direction. Upper part bcc: matrix; lower part: B2 inclusion.

centre of the micrograph and is rather sharp. In the upper part of the image, the typical pattern corresponding to the (1 1 0) projection of the bcc structure is seen. The contrast is very homogeneous, and there is no indication of short- or medium-range order. The lower part of the image, corresponding to the inclusion, clearly shows the presence of B2 ordering: every other atomic row corresponding to a (0 0 1) plane is significantly darker in contrast, which demonstrates the occupation of the corresponding atomic positions by lighter atoms.

Figure 4(d) also demonstrates that the phase boundary between the bcc and B2 phase is perfectly coherent. The lattice parameter according to STEM is about 2.9 nm for the bcc as well as the B2 phase, and all lattice planes pass through the phase boundary without any disturbance—the lattices of the two phases are aligned and in perfect registry. Accordingly, the selected-area diffraction patterns (Figure 3), which originate from a diffraction volume containing bcc and B2 phase as well as several phase boundaries, display only a single set of reflections and are undistorted and sharp. The same holds for Laue diffraction, which corresponds to an even larger diffracting volume. Hence, the entire primary grain contains a single consistent and continuous set of lattice planes, and can be referred to as a single crystal, even though two phases of different chemistry and order are present. As such, the situation, for example, accords with that of Ni-based superalloy single crystals [9,10].

The two-phase structure is similar to that of equiatomic AlCoCrFeNi HEAs, where the presence of bcc and B2 phases was also found [11]. However, the matrix/inclusion setting is inverted: while the FeCoCrMnAl HEA presented

in this study has a bcc matrix and B2 inclusions, in AlCoCrFeNi HEAs the matrix is B2 ordered and the inclusions are bcc.

The Bridgman technique employed is a near-equilibrium growth method. The applied growth velocity is low and the grown crystal is cooled very slowly, which implies that the solidified material is annealed for several hours. We therefore conclude that the material is well equilibrated and the described two-phase structure is thermodynamically stable. Its formation may take place similar as in AlCoCrFeNi HEAs, where the two-phase structure forms by spinodal decomposition [11].

We have furthermore analysed the chemical composition of the matrix and the inclusions. Figure 5 shows a HAADF STEM micrograph along with EDX-spectroscopy maps of the same sample area. In the HAADF STEM micrograph the bcc matrix is imaged bright, and the B2 inclusions are dark. As can be seen from the EDX-spectroscopy maps, the inclusions predominantly contain Al and Co, while the matrix is rich in Fe and Cr. Mn is present in both phases but more predominant in the matrix. The quantitative compositions for the two phases according to EDX spectroscopy are $Fe_{22}Co_6Cr_{44}Mn_{20}Al_8$ for the matrix and $Fe_{15}Co_{34}Cr_5Mn_{13}Al_{33}$ for the B2 inclusions (with an assumed absolute error of about ±5%).

In conclusion, in this paper we demonstrate the successful growth of single crystals of an HEA of the equiatomic phase FeCoCrMnAl. The crystal analysed consists of a primary grain and two small secondary grains. The volume of the primary grain is 4.8 cm^3. To the best of our knowledge this is the first report of the successful growth of a cubic-centimetre-sized single crystal of an HEA.

The availability of single-crystalline sample materials is highly important for the determination of intrinsic materials properties without stray influences of the results by grain boundaries or other impurities. Furthermore, large samples are demanded by several characterization techniques such as neutron scattering, requiring sample volumes of the order of 1 cm^3, surface investigation techniques such as scanning tunnelling microscopy combined with low-energy electron diffraction, and corrosion and tribology studies, requiring sample surface areas of several tens of mm^2 and lateral sample surface extensions of up to 10 mm. Further examples are low-frequency elastic constant measurements and anelasticity measurements with a torsion pendulum, etc. Neutron scattering for the determination of short- and medium-range order is of particular importance in HEAs: most HEA phases include atom species which are closely neighboured in the periodic table, thus having very

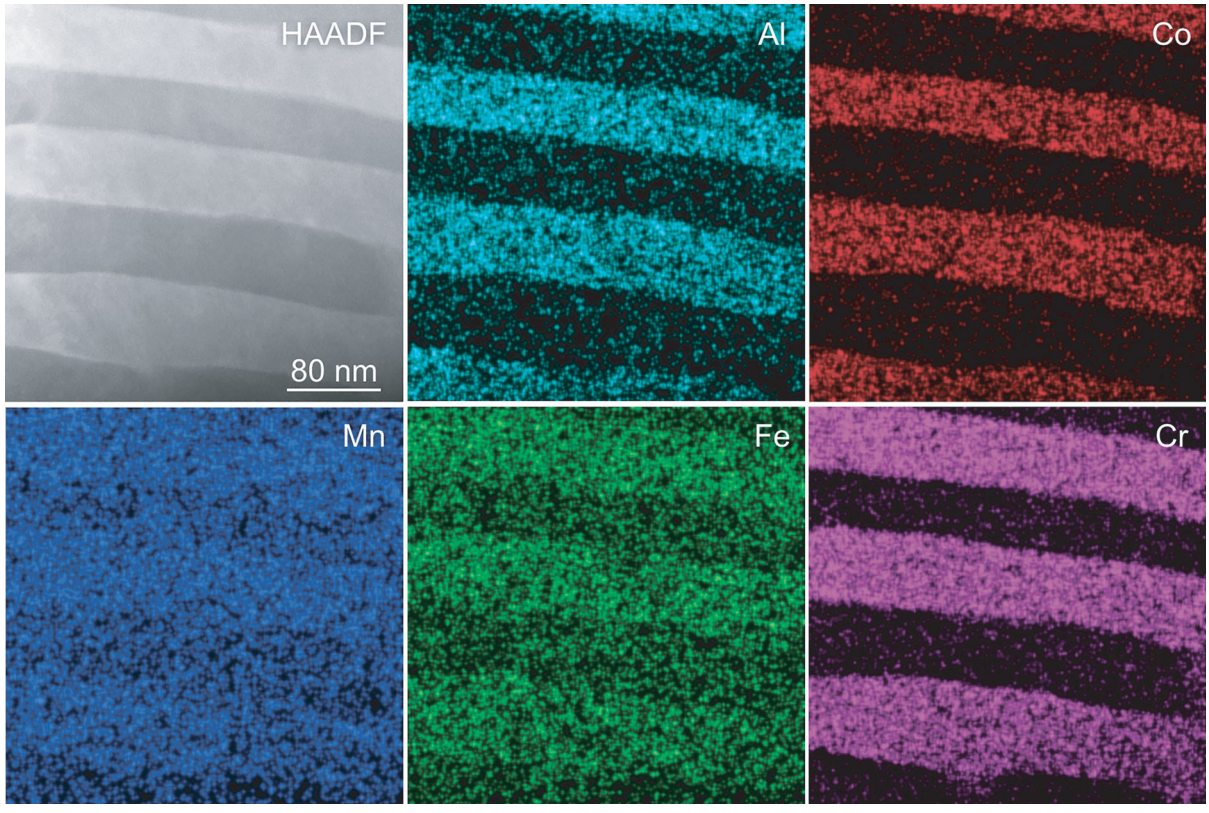

Figure 5. HAADF STEM micrograph and EDX-spectroscopy maps of the elements included.

similar atomic numbers. As a result, X-ray and electron diffraction techniques will suffer from a lack of contrast and thus may be only of limited use for structural studies of these materials. It is also conceivable that FeCoCr-MnAl single crystals possess physical properties that are different and potentially superior to those of polycrystalline material. Of particular interest in this respect are the mechanical properties, as, for example, for Ni_3Al superalloys, which in single-crystalline form exhibit twice the yield strength of polycrystalline material [10].

There is one previous publication on single-crystal growth of an HEA [5]. It reports on the growth of a single crystal in the system $CoCrFeNiAl_{0.3}$ by means of a Bridgman technique. The crystal grown, however, is only 3 mm in diameter at a length of 50 mm. Its total volume is thus only 0.35 cm^3 and therewith only allows for a limited range of experimental approaches.

Our study shows that single-crystal growth of HEAs up to a size of several cm^3 is feasible. The size of the single crystal presented in this study is limited by the crucible used. The growth of even larger crystals, if required, seems achievable. In a next step, we will survey the consequences of the growth parameters such as the lowering velocity, the growth temperature, and temperature gradients on the resulting crystal, and we will approach the growth of oriented single crystals using the seeded Bridgman or the Czochralski technique. Furthermore, we are on the verge of developing single-crystal growth routes of related HEAs such as face-centred cubic FeCoCrMnNi and FeCoCrMnPd, in order to allow comparative studies of physical properties, which will allow a deeper insight into the structure–property relations of this class of materials.

Acknowledgements

The authors thank K.G. Pradeep and A. Marshal for disclosing their discovery of the FeCoCrMnAl HEA to us prior to publication, and M. Heggen for additional TEM investigations.

Disclosure statement

No potential conflict of interest was reported by the authors.

References

[1] Yeh JW, Chen SK, Lin SJ, et al. Nanostructured high-entropy alloys with multiple principal elements: novel alloy design concepts and outcomes. Adv Eng Mater. 2004;6:299–303.
[2] Cantor B, Chang ITH, Knight P, et al. Microstructural development in equiatomic multicomponent alloys. Mater Sci Eng A. 2004;375–377:213–218.
[3] Feuerbacher M, Heidelmann M, Thomas C. Hexagonal high-entropy alloys. Mater Res Lett. 2015;3:1–6.
[4] Marshal A, Pradeep KG, Music D, et al. Combinatorial synthesis of high entropy alloys: Introduction of a novel, single phase, body-centered-cubic FeMnCoCrAl solid solution. J Alloys Compd. 2016. doi:10.1016/j.jallcom.2016.08.326
[5] Ma SG, Zhang SF, Gao MC, et al. A successful synthesis of the CoCrFeNiAl0.3 single-crystal, high-entropy alloy by Bridgman solidification. JOM 2013;65:1751–1758.
[6] Ernst Ruska-Centre for Microscopy and Spectroscopy with Electrons. FEI Helios NanoLab 400S FIB-SEM. J Large Scale Res Facil. 2016;2:1–4.
[7] Ernst Ruska-Centre for Microscopy and Spectroscopy with Electrons. FEI Titan G2 80-200 CREWLEY. J Large Scale Res Facil. 2016;2:1–4.
[8] Feuerbacher M, Würtz E, Thomas C. Single-crystal growth of a FeCoCrMnAl high-entropy alloy. arXiv:1606.09476.
[9] Caron P, Khan T. Evolution of Ni-based superalloys for single crystal gas turbine blade applications. Aerosp Sci Technol. 1999;3:513–523.
[10] Golberg D, Demura M, Hirano T. Single crystal growth and characterization of binary stoichiometric and Al-rich Ni_3Al. J Cryst Growth. 1998;186:624–628.
[11] Manzoni A, Daoud H, Völkl R, et al. Phase separation in equiatomic AlCoCrFeNi high-entropy alloy. Ultramicroscopy. 2013;132:212–215.